BMC Plant Biology

RESEARCH Open Access

Revisiting the phylogeny of *Conioselinum* (Apiaceae) by integrating nrDNA, plastomes and morphology evidence

Meng-Die Liu[1], Xing-Jin He[1], Zi-Xuan Li[1], Wei-Yan Tan[1], Deng-Feng Xie[1], Ting Ren[1,2], Bo-Ni Song[1] and Song-Dong Zhou[1*]

Abstract

Background The genus *Conioselinum* Fisch. ex Hoffm. (Apiaceae) presents long-standing taxonomic challenges due to poorly resolved infrageneric relationships and significant morphological convergence with related genera such as *Ligusticum* s.l. Although integrating plastomes and nrDNA data has been effective in resolving complex phylogenies, a comprehensive phylogenetic framework and a critical reevaluation of key diagnostic traits for *Conioselinum* remain insufficient.

Results Our nrDNA phylogeny established a robust framework supporting the monophyly of *Conioselinum* as nested within the *Hymenidium* clade, delineating three distinct subclades (A, B, and C). This phylogenetic framework is further corroborated by corresponding morphological traits. We reaffirmed that the terminal localization of vascular bundles in fruit ribs is a stable synapomorphy for *Conioselinum*, when integrated with a consistent suite of diagnostic markers—specifically deciduous basal leaves, linear bracteoles, and absent or obsolete calyx teeth—it effectively distinguishes the genus from closely related allies. Divergence time estimation traced a rapid radiation from the Late Miocene to the Pleistocene, coinciding with the Qinghai-Tibet Plateau uplift. Furthermore, selective pressure analyses identified positive or relaxed selection in six genes (*ycf1*, *matK*, *rpoA*, *ycf2*, *rps7*, and *ccsA*), suggesting their role in adapting to alpine environmental stresses. Evident cytonuclear conflicts in some taxa underscore a complex history likely involving reticulate evolution.

Conclusion This study highlights the utility of integrating phylogenomics with morphology to resolve complex taxonomies. Based on congruent evidence from both sources, we propose a revised circumscription for *Conioselinum*. Together, these molecular and morphological insights establish a solid foundation for future taxonomic revisions and enhance our understanding of adaptive diversification in Apiaceae.

Keywords Apiaceae, Conioselinum, Plastome, Morphology, Phylogeny, Integrative taxonomy

*Correspondence:
Song-Dong Zhou
zsd@scu.edu.cn
[1]Key Laboratory of Bio-Resource and Eco-Environment of Ministry of Education, College of Life Sciences, Sichuan University, Chengdu 610065, China
[2]Xi'an Botanical Garden of Shaanxi Province (Institute of Botany of Shaanxi Province), Xi'an 710061, China

Background

The genus *Conioselinum* Fisch. ex Hoffm. (Apiaceae) was established by Georg Franz Hoffmann in 1814, with *Conioselinum tataricum* Hoffm. designated as the type species in 1816. The genus is morphologically characterized by persistent and numerous bracts, obcordate petals, and ovate fruits with winged ribs and multiple commissural vittae [1]. Although initially monotypic (*C. tataricum*), *Conioselinum* has undergone extensive taxonomic revisions over the past two centuries. These modifications include the addition of 8 to 9 species, the exclusion of several taxa [2, 3], and the transfer of ten species formerly placed in *Ligusticum* s.l. and two from *Cnidium* Cusson [4, 5] (Fig. 1, Table S1). Despite these efforts, the circumscription of *Conioselinum* remains contentious due to discrepancies across various floristic accounts. While

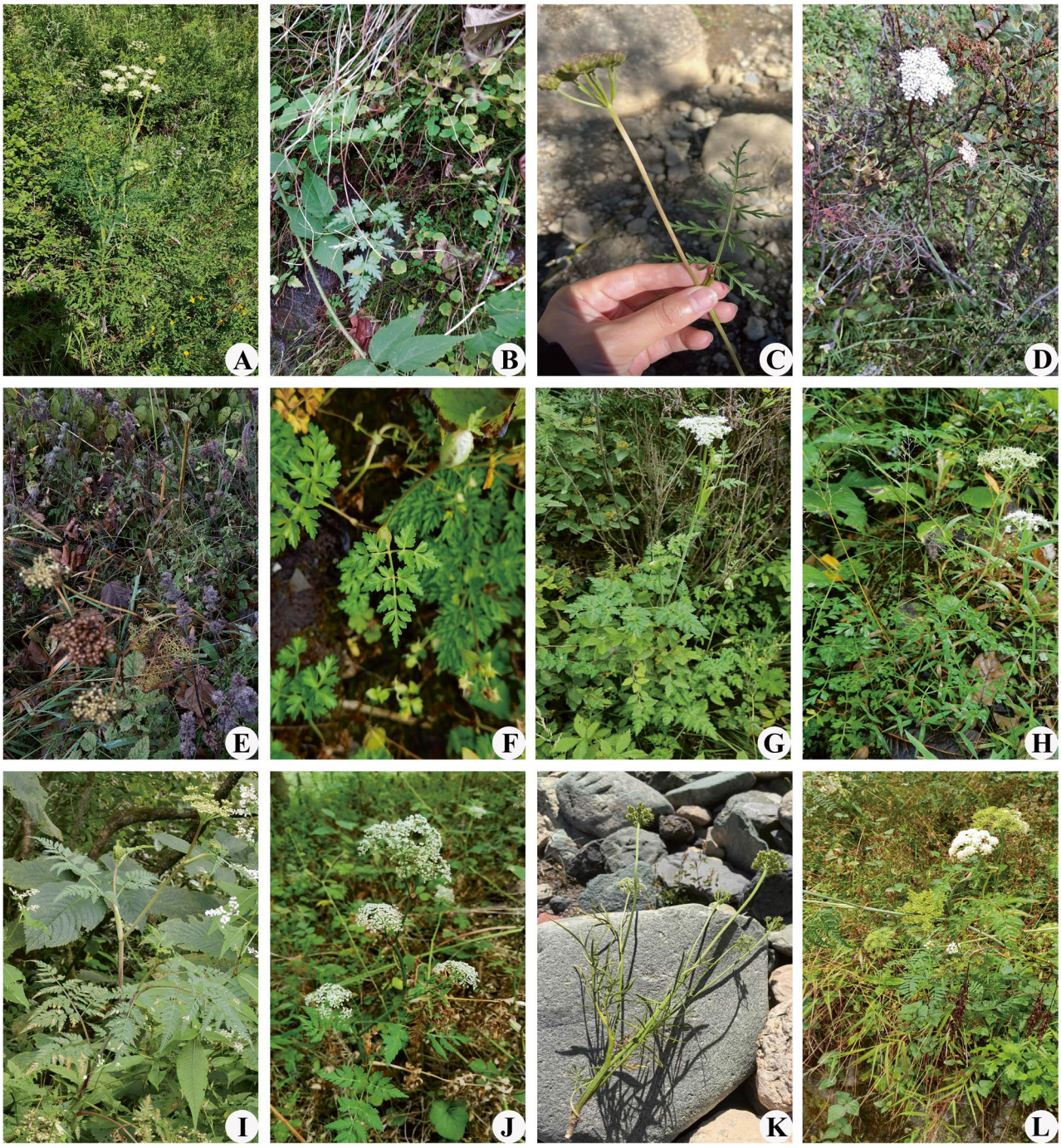

Fig. 1 Images of 12 taxa under *Conioselinum*. **A** *Conioselinum tataricum*, the type of *Conioselinum*; **B** *C. shanii*; **C** *C. reflexum*; **D***C. nematophyllum*; **E***C. tenuisectum*; **F**. *Liguticum reptans*; **G**. *C. smithii*; **H**. *C. pteridophyllum*; **I**. *C. acuminatum*; **J**. *C. anthriscoides*; **K**. *Kadenia salina*; **L**. *C. nullivittaetum*

maintained as a distinct genus in the floras of Northern/Central Europe, Northern Asia, and North America [6–8], it is frequently merged within *Ligusticum* s.l. in treatments focusing on central and southwestern China [9–11]. This taxonomic instability stems largely from the striking morphological convergence between *Conioselinum* and *Ligusticum* s.l., particularly regarding their highly dissected leaves and the presence of winged lateral ribs in the mericarps, underscoring the urgent need for an integrated systematic re-evaluation utilizing robust molecular and morphological evidence.

Significant gaps persist in the understanding of this taxonomically complex group. Early molecular study using the *rbcL* gene suggested a close relationship between *Conioselinum filicinum* (Wolff) Hara and a cluster comprising *Cnidium officinale* Makino., *Ligusticum sinense* Oliv., and *Ligusticum jeholense* (Nakai & Kitag.) Nakai & Kitag [12]. Subsequent analyses of nuclear ribosomal internal transcribed spacer (nrITS, including ITS1 and ITS2) sequences revealed that *Conioselinum* species are nested within the *Hymenidium* (*Sinodielsia*) clade and the *Conioselinum chinense* clade. Notably, previous researchers have hypothesized that the latter might represent misidentified specimens of *C. chinense* [13–15]. To date, phylogenetic insights into the genus have been derived from studies characterized by specific taxon sampling and identified instances of paraphyly, providing a foundational but partial understanding of intrageneric relationships. While traditional DNA barcodes such as *rbcL*, *matK*, and nrITS have been instrumental in early broad-scale analyses, their resolution within lineages exhibiting low substitution rates remains to be fully explored. Regarding morphological evidence, although extensive documentation exists for general fruit anatomy, these data have yet to be rigorously evaluated within a phylogenomic framework to assess character evolution; meanwhile, other key features, including pollen morphology [16–18], leaf epidermis [19–21], and cytological characteristics [22, 23], represent areas that await further comprehensive investigation.

To resolve these taxonomic ambiguities, we employed next-generation sequencing (NGS) technologies. Genome skimming has emerged as a powerful tool for resolving complex phylogenies by providing high-density genomic data. By simultaneously capturing both plastome data and complete nuclear ribosomal DNA (nrDNA, including the ETS, 18 S, ITS1, 5.8 S, ITS2, 26 S, and partial NTS regions), this approach provides a wealth of phylogenetically informative sites. Such comprehensive genomic resources offer significantly higher resolution for resolving evolutionary relationships than individual gene fragments or traditional molecular markers [24–32].

In this study, we integrate plastomes, nrDNA sequences and carpological evidence to revisit the phylogeny of *Conioselinum*. Our specific objectives were to: (i) reconstruct a robust phylogenetic framework for *Conioselinum* and its allies by integrating molecular data with morphological traits to clarify long-standing inter- and infrageneric taxonomic uncertainties; (ii) compare the structural characteristics and adaptive evolution of *Conioselinum* plastomes to understand the genomic basis of their diversification. By prioritizing phylogenetic resolution over broad genomic description, this study aims to provide a more definitive taxonomic understanding of *Conioselinum* within the family Apiaceae.

Results

Characteristics of NrDNA and plastomes

The assembled nrDNA sequences and plastomes of 16 representative taxa (14 *Conioselinum* species and two close biological allies) were analyzed to assess genomic conservation and divergence. The nrDNA sequence of each sample was composed of six regions: ETS, 18 S, ITS1, 5.8 S, ITS2, 26 S+partial NTS), ranging from 7,054 bp (*Ligusticum reptans* (Diels) H.Wolff) to 10,672 bp (*Conioselinum nematophyllum* Pimenov & Kljuykov). The GC content of each complete nrDNA sequence is observed to range from 51.8% to 53.3% (Table 1). While the GC content in the transcription region remains relatively stable: the GC content in the 18 S region (49.0%–49.1%); 5.8 S region (53.8%–54.4%); and 26 S+partial NTS region (52.7%–54.9%).

The plastomes exhibited a typical quadripartite structure, ranging from 135,088 bp (*Conioselinum reflexum* Pimenov & Kljuykov) to 158,320 bp (*Kadenia salina* (Turcz.) Lavrova & V.N.Tikhom.), with a CG content of 36.8% to 37.6%. While gene content was largely consistent (121–134 genes), significant gene losses (*rrn23*, *rrn16*, *ycf15*, *ycf68*, *rps7*, *ndhB*, *trnA-UGC*, *trnI-GAU*, *trnL-CAA*, and *trnV-GAC*) were identified in *C. reflexum*, and localized duplications (*trnK-UUU*, *matK*, and *psbA*) were observed in *K. salina* (Table 2 and S2, Fig. 2). Analysis of IR/SC boundaries revealed that the JSA and JSB borders were relatively stable, positioned within the *ycf1* and retro-copy *ycf1* (*ψycf1*) regions, with a fixed distance of 1886 bp (*ψycf1* to JSB, JSA to *ycf1*) across all plastomes (Figure S1, marked in red). In contrast, the JLB boundary was variable, positioned within *ycf2*, *trnH* (in *C. tataricum*), or *rrn23* (in *C. reflexum*). Notably, the JLA line exhibited between the *trnL* and *trnH*, but *C. reflexum* and *K. salina* exhibited IR contraction and expansion, respectively, affecting the JLA boundary. Although RSCU values were generally conserved across the genus (Figure S2, Table S3), sequence divergence analysis highlighted specific hypervariable coding regions (*ycf1*, *ycf2*, *rps19*, and *psbE-psbJ*) (Figure S3 and S4). These results underscore

Table 1 Summarizes the main features of the NrDNA sequences among 16 sampled species of *Conioselinum* and its close biological allies

Species	nrDNA													
	Total Length (bp)	Total GC%	ETS		18 S		ITS1		5.8 S		ITS2		26 S+partial NTS	
			Length (bp)	GC%	Length (bp)	GC%	Length (bp)	GC%	Length (bp)	GC%	Length (bp)	GC%	Length (bp)	GC%
Conioselinum tataricum	7822	53.2	477	52.8	1809	49.1	217	56.2	160	55.0	224	55.4	4935	54.5
Conioselinum nematophyllum	10,672	52.7	477	50.9	1809	49.1	219	55.7	160	55.0	225	56.0	7782	53.4
Conioselinum sinchianum	7746	53.0	578	50.2	1809	49.1	218	55.5	160	55.0	225	56.0	4756	54.5
Conioselinum acuminatum	10,532	52.7	564	50.4	1809	49.0	218	56.0	160	55.0	225	56.0	7556	53.5
Conioselinum nullivittaetum	10,665	53.3	478	50.4	1809	49.0	218	54.6	160	54.4	225	56.0	7775	54.4
Conioselinum tenuisectum	10,423	52.8	478	50.6	1809	49.0	218	54.1	160	54.4	225	56.0	7533	53.7
Conioselinum smithii	10,228	51.9	478	50.2	1809	49.1	217	55.3	160	54.4	224	54.5	7340	52.5
Conioselinum anthriscoides	7202	52.6	478	50.2	1809	49.1	217	55.3	160	54.4	224	54.5	4314	54.0
Conioselinum shanii	8719	52.0	478	50.2	1809	49.1	217	55.3	160	54.4	224	54.5	5831	52.8
Conioselinum tenuissimum	7502	53.2	478	50.2	1809	49.1	217	55.3	160	54.4	224	54.5	4614	54.9
Conioselinum officinale	6827	52.6	478	50.2	1809	49.1	217	55.3	160	54.4	224	54.5	3939	54.1
Conioselinum pseudoangelica	10,137	52.2	477	50.9	1809	49.1	217	54.8	160	53.8	225	54.2	7249	52.9
Conioselinum pteridophyllum	8874	51.8	586	50.2	1809	49.1	217	55.8	160	53.8	225	54.7	5877	52.6
Conioselinum reflexum	9764	52.3	477	51.2	1809	49.1	217	55.3	160	53.8	225	54.2	6876	53
Kadenia salina	10,299	52.1	478	50.4	1809	49.0	218	55.0	160	55.0	225	54.7	7409	52.7
Ligusticum reptans	7054	52.3	478	50.0	1809	49.0	217	55.3	160	54.4	224	54.5	4166	53.6

the overall structural stability of *Conioselinum* plastomes while identifying lineage-specific variations that provide the basis for subsequent phylogenetic and marker screening analyses.

Phylogenetic relationships

Phylogenetic analyses of 45 taxa based on nrDNA and plastome protein-coding genes (CDS) sequences yielded well-supported but strongly incongruent topologies (Fig. 3). In the nrDNA phylogeny, 16 taxa (14 *Conioselinum* species and two close biological allies) formed a monophyletic group (ML bootstrap values, BS = 90; BI posterior probabilities PP = 0.87), corresponding to the *Hymenidium* clade. This clade was sister to a clade containing genera such as *Angelica* L., *Hymenidium* Lindl., *Trachydium* Lindl., *Levisticum* Hill, *Seselopsis* Schischk., and *Oreocomopsis* Pimenov & Kljuykov. These 16 taxa were further resolved into three subclades with high support. Subclade A (BS = 99; PP = 1) is regarded as the core *Conioselinum* clade, as it contains the type species, *C. tataricum*, along with six other species: *Conioselinum nematophyllum* Pimenov & Kljuykov, *Conioselinum acuminatum* (Franch.) Lavrova, *Conioselinum sinchianum* (Fu Kuntsun) Pimenov & Kljuykov, *Conioselinum nullivittatum* (K. T. Fu) T. Ren & X. J. He, *Conioselinum tenuisectum* (H. Boissieu) Pimenov & Kljuykov, and *K. salina*. The remaining species were divided into two sister subclades: subclade B (BS = 100; PP = 1), comprised three species (*C. reflexum*, *Conioselinum pseudoangelica* (H.Boissieu) Pimenov & Kljuykov, and *Conioselinum pteridophyllum* (Franch.) Lavrova). Subclade C (BS = 100; PP = 1) consisted of the six remaining species (*Conioselinum shanii* Pimenov & Kljuykov, *Conioselinum anthriscoides* (H.Boissieu) Pimenov & Kljuykov., *Conioselinum smithii* (H.Wolff) Pimenov & Kljuykov, *Ligusticum reptans* (Diels) H. Wolff, *Conioselinum tenuissimum* (Nakai) Pimenov & Kljuykov, and *Conioselinum officinale* (Makino) K.Ohashi & H.Ohashi).

In contrast, the plastome CDS phylogeny exhibited a strong topological conflict with the nrDNA tree. The topology of the phylogenetic trees constructed by the concatenation method and ASTRAL is consistent (Figure S5). Specifically, a significant and well-supported incongruence was observed regarding the position of the type species, *C. tataricum*, which was recovered as an independent lineage sister to a large clade comprising other species of Subclade A and Subclade C (BS = 100; PP = 1). More strikingly, all three species of subclade B, together with *K. salina*, formed a distinct clade (BS = 100; PP = 1) that was sister to a larger assemblage including the *Hymenidium* clade, Selineae and Coriandreae (BS = 100; PP = 1). This positioning represents a hard topological conflict compared to the nrDNA framework, supported by maximum bootstrap and posterior probability values in both analyses.

Morphological and anatomical evidence

Based on field observations, herbarium reviews, and detailed anatomical analysis of 16 representative taxa, the studied group exhibits high logical congruence with the nrDNA phylogenetic framework (Fig. 4). By plotting these alternative character states against the nrDNA tree, we confirmed that while the terminal position of vascular bundles remains a stable synapomorphy for the genus

Table 2 Summary of plastome genomic features among 16 sampled species of *Conioselinum* and its close biological allies

Species	Length (bp)				Gene Number				GC (%)
	Total	LSC	SSC	IRs	Total	PCG	tRNA	rRNA	
***Conioselinum tataricum*(Type species)**	148,642	93,747	17,665	37,230	130	85	36	8	37.6
Conioselinum nematophyllum (= *Ligusticum nematophyllum*)	148,610	94,007	17,635	36,968	130	85	36	8	37.6
Conioselinum sinchianum (= *Cnidium sinchianum*)	148,652	94,014	17,676	36,962	130	85	36	8	37.6
Conioselinum acuminatum (= *L. acuminatum*)	148,005	93,314	17,701	36,990	130	85	36	8	37.6
Conioselinum nullivittaetum (= *L. nullivittaetum*)	148,590	93,969	17,653	36,968	130	85	36	8	37.6
Conioselinum tenuisectum (= *L. tenuisectum*)	148,356	93,725	17,653	36,978	130	85	36	8	37.6
Conioselinum smithii (= *L. jeholense*)	148,489	93,889	17,642	36,958	130	85	36	8	37.6
Conioselinum anthriscoides (= *L. sinense*)	148,520	93,957	17,613	36,950	130	85	36	8	37.6
Conioselinum tenuissimum (= *L. tenuissimum*)	148,553	93,979	17,632	36,942	130	85	36	8	37.6
Conioselinum pseudoangelica (= *L. glaucifolium*)	146,985	94,350	17,513	35,112	130	85	36	8	37.5
Conioselinum pteridophyllum (= *L. pteridophyllum*)	147,500	94,865	17,513	35,122	130	85	36	8	37.4
Conioselinum officinale (= *Cnidium officinale*)	148,564	94,011	17,617	36,936	130	85	36	8	37.6
Conioselinum shanii	148,487	93,955	17,608	36,924	130	85	36	8	37.6
Conioselinum reflexum	135,088	106,488	17,514	11,086	121	81	33	6	36.8
Kadenia salina	158,320	88,766	17,598	51,956	134	87	38	8	37.0
Ligusticum reptans	148,540	93,992	17,584	36,964	130	85	36	8	37.6

i) Species *Kadenia salina* and *Ligusticum reptans* are included due to their robust phylogenetic affinity to *Conioselinum* based on preliminary molecular data

ii) PCG: Protein-coding gene

Conioselinum, traits such as bract persistence, petal color, and fruit rib morphology provide the most reliable diagnostic markers for infrageneric delimitation.

At the intergeneric level, the localization of vascular bundles within the fruit ribs is confirmed as a definitive diagnostic synapomorphy distinguishing *Conioselinum* from its closely related genera (such as *Angelica*, *Hymenidium*, *Oreocomopsis*, and *Levisticum*). Specifically, all examined *Conioselinum* species and two close biological allies stably possess vascular bundles at the terminal position of the ribs, whereas they are consistently situated at the base in outgroup genera (Figure S6). Furthermore, the endosperm shape serves as a differentiating trait: *Conioselinum* species typically possess narrowly elliptic or elliptic endosperm, contrasting with the U-shaped endosperm with a significant depression characteristic of *Hymenidium* and *Oreocomopsis* (Tables S4).

At the infrageneric level, distinct alternative character states across the three identified subclades demonstrate a clear evolutionary trajectory. A primary transition is evident in the bract and bracteole morphology: Subclades A and B are characterized by caducous or absent bracts and linear bracteoles, whereas Subclade C is uniquely distinguished by persistent bracts and linear bracteoles with prominent white-membranous margins. Petal coloration further differentiates these lineages, with white petals being standard for Subclades A and C, while colorful or purplish hues frequently occur in Subclade B (Tables S5). In terms of carpology, mericarp morphology shifts from the oblong-obovate shape with broad-winged marginal ribs typical of Subclades A and B to an ovate shape with significantly reduced marginal ribs in Subclade C. Furthermore, the number of commissural vittae serves as a distinctive anatomical marker, with Subclade B typically possessing a higher count (up to six) compared to the more stable range of two to four observed in Subclade A (Fig. 4, Tables S4).

Plastome divergence

To understand the evolutionary constraints on the *Conioselinum* plastomes, we analyzed nucleotide diversity (Pi) (Figure S7) and the Ka/Ks ratio (ω) (Figure S8) across the sixteen representative taxa. The Pi analysis of 53 CDS regions and 65 intergenic spacers revealed that non-coding regions exhibited significantly higher variability (mean Pi = 0.00595, up to 0.03621 in *ccsA-ndhD*) compared to CDS regions (mean Pi = 0.00225). Based on these results, we identified seven highly variable genomic hotspots, including five CDS regions (Pi > 0.005): *matK*, *rps2*, *rps3*, *ycf2*, and *ycf1*, and 2 intergenic spacers (Pi > 0.015): *ccsA* | *ndhD* and *petA* | *psbJ*, which are proposed as candidate molecular markers for future large-scale species identification and phylogenetic studies in this genus.

Consistent with the low sequence divergence in coding regions, the Ka/Ks analysis indicated that most genes are under widespread purifying selection (ω < 1) [33]. However, the *ycf1* gene exhibited an ω value greater than 1 (1.09268), suggesting it has undergone positive selection. Additionally, five genes (*matK*, *rpoA*, *ycf2*, *rps7*, and *ccsA*) showed elevated ω values exceeding 0.5. The coincidence of high Pi values and relaxed evolutionary constraints in genes like *ycf1*, *ycf2*, and *matK* further underscores their potential utility as phylogenomic markers, reflecting the rapid diversification and adaptive evolution of *Conioselinum*.

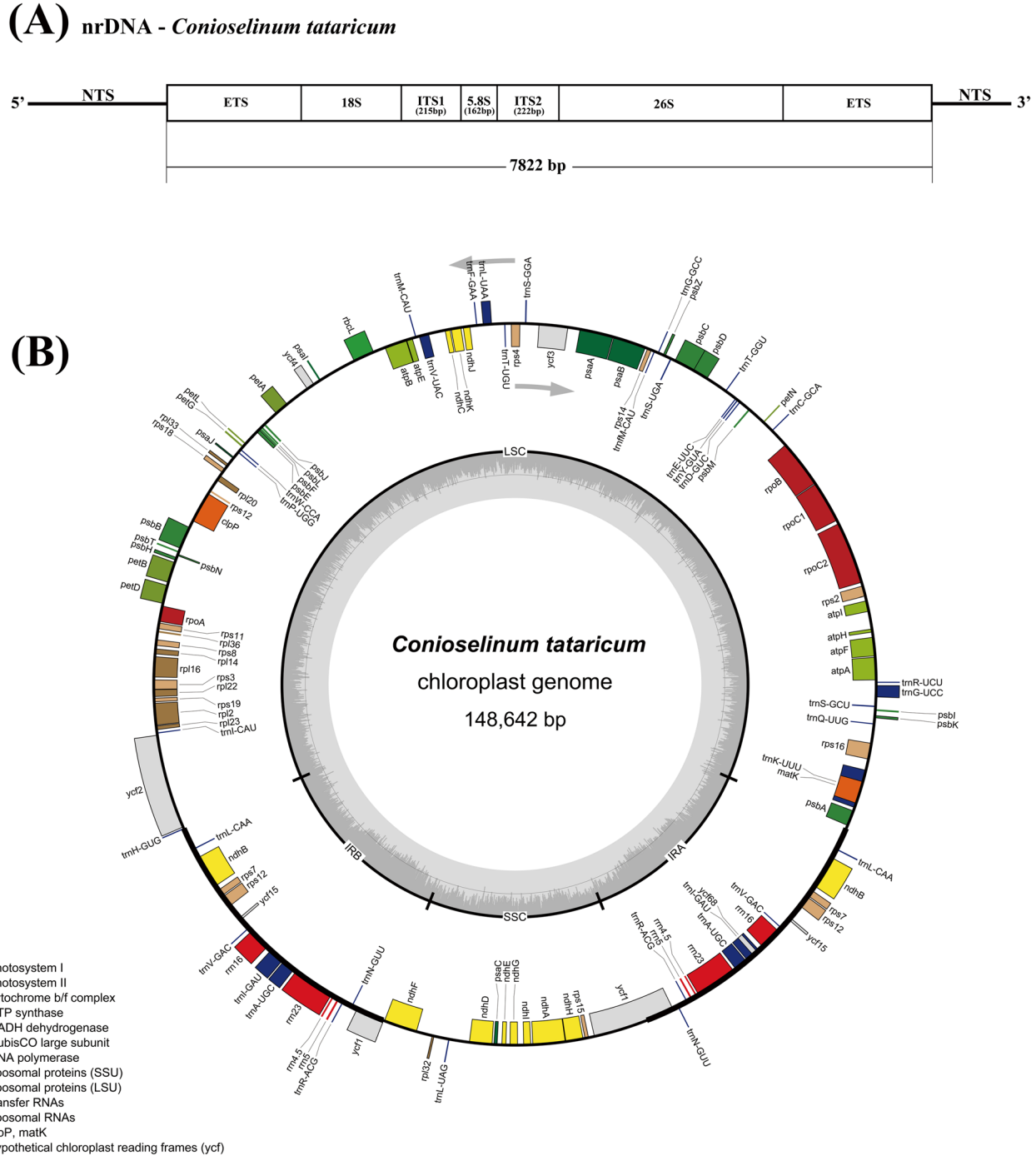

Fig. 2 Genomic characteristics of the type species *Conioselinum tataricum*. **A** Schematic diagram of the nuclear ribosomal DNA (nrDNA) structure. ETS: External Transcribed Spacer, 18 S rRNA, ITS1 and 2: Internal Transcribed Spacer Regions 1 and 2, 5.8 S rRNA and 26 S rRNA, flanked by Non-Transcribed Spacers (NTS). The lengths of specific regions are indicated in parentheses. **B** Map of the chloroplast genome. LSC: Large Single-Copy region, SSC: Small Single-Copy region, and IRa and IRb: Inverted Repeats a and b. The gray bars in the inner circle represent GC content

Divergence time Estimation

Divergence times were estimated using the MCMCTree method based on two molecular datasets: nrDNA (Fig. 5) and plastome 79 CDS (Table S6). The analysis inferred that the *Hymenidium* Clade diverged from the Selineae–Coriandreae clade during the Miocene, with estimates ranging from approximately 16.44 Mya (95% HPD: 5.61–30.58 Mya) based on nrDNA to 8.8 Mya (95% HPD: 2.27–19.9 Mya) based on the plastome. Significant temporal asymmetry was observed regarding the origin of the genus *Conioselinum*. The nrDNA data estimated this origin at approximately 12.58 Mya (95% HPD: 4.25–24.05

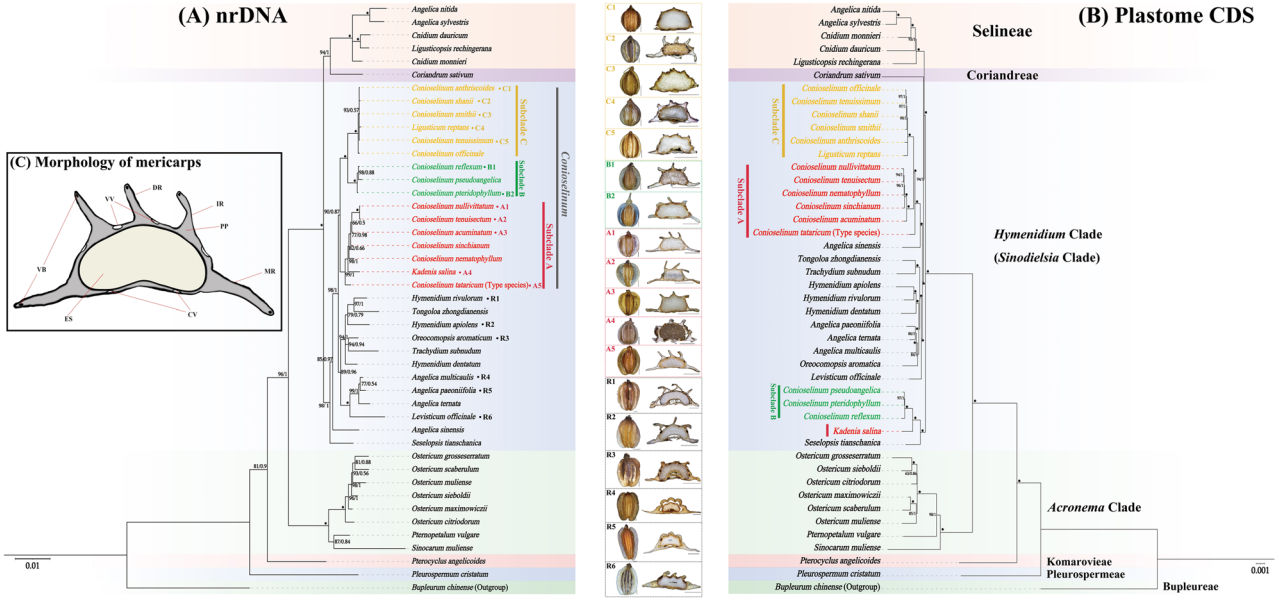

Fig. 3 Combination of mericarps and phylogenetic phylogenetic tree, reconstructed using both (**A**) maximum likelihood (ML) and (**B**) Bayesian inference (BI) analyses based on nrDNA and plastome CDS sequences for 45 taxa. *Conioselinum* comprising three major subclades: Subclade A (red), Subclade B (green), and Subclade C (yellow). Branch supports are indicated as bootstrap values (BS) for ML and posterior probabilities (PP) for BI, asterisks (*) denote maximal support (BS = 100%, PP = 1); (**C**) Typical mericarp structure of *Conioselinum*, vascular bundles (VB); endosperm (ES); dorsal ribs (DR), lateral ribs (LR), marginal ribs (MR); parenchyma cells with lignified pitted walls (PP), furrow vittae (VV), and the commissure vittae (CV); Scale bars = 1 mm

Mya), while the plastome data provided a more recent estimate of approximately 6.84 Mya (95% HPD: 1.72–15.75 Mya).

In the nrDNA phylogeny, Subclade A diverged during the late Miocene, while Subclades B and C split approximately 6.56 Mya (95% HPD: 1.84–14.53 Mya). Most *Conioselinum* species diversified and formed after the Miocene, with the majority of extant species diversifications occurring during the Quaternary, with the notable exceptions of the initial splits leading to *C. tataricum* and *K. salina*. Within the *Hymenidium* clade, the plastome analysis identified a major divergence event around 7.18 Mya (95% HPD: 1.74–16.95 Mya), leading to a lineage comprising *K. salina* and the species of Subclade B.

Discussion

Plastome evolution and adaptive divergence

A comparative analysis of 16 plastomes (including 14 *Conioselinum* taxa and 2 closely related allies) reveals a conserved genomic architecture punctuated by specific instances of structural dynamism. All investigated plastomes exhibit the quadripartite structure typical of Apiaceae (Fig. 2; Table 2) [34–37]. Nevertheless, conspicuous structural modifications were identified in *C. reflexum*, characterized by gene loss and IR contraction, and in *K. salina*, which displays genome expansion driven by gene duplication and IR expansion. Such rearrangements are frequently concomitant with phylogenetic discordance [38, 39], providing a plausible genomic basis for the incongruent phylogenetic placements of these taxa between plastome and nuclear datasets.

Interestingly, this structural plasticity contrasts with the high conservation observed in features such as codon usage, suggesting an evolutionary decoupling where architectural rearrangements occur independently of synonymous substitution patterns. This genomic stability amidst structural shifts may be a byproduct of the genus's broad environmental tolerance. Distributed widely across East Asia to North America, *Conioselinum* species predominantly span temperate zones above 1500 m, facing diverse selective pressures from high-light arid slopes to moist, shaded alpine habitats (Figs. 1 and 4) [10].

To identify the genetic signatures underlying this environmental adaptation, we analyzed selective pressures on 53 PCGs (> 300 bp). While the majority of these genes are under stringent purifying selection ($\omega < 0.5$), the identified positive selection on *ycf*1 ($\omega > 1.0$) is particularly noteworthy. Given its essential role in cell survival, the positive selection of *ycf1* may have bolstered resilience to alpine abiotic stresses, such as elevated UV radiation and extreme temperature fluctuations [40]. Additionally, we detected evidence of relaxed purifying selection ($0.5 < \omega < 1$) on five genes (*matK*, *rpoA*, *ycf2*, *rps7*, and *ccsA*). The relaxed selection on *rpoA* (RNA polymerase subunit) and *rps7* (ribosomal protein) suggest a capacity for functional diversification or compensatory evolution in chloroplast transcription and translation [41–43], while shifts in *ccsA* (cytochrome biogenesis), *matK* (intron maturase), and

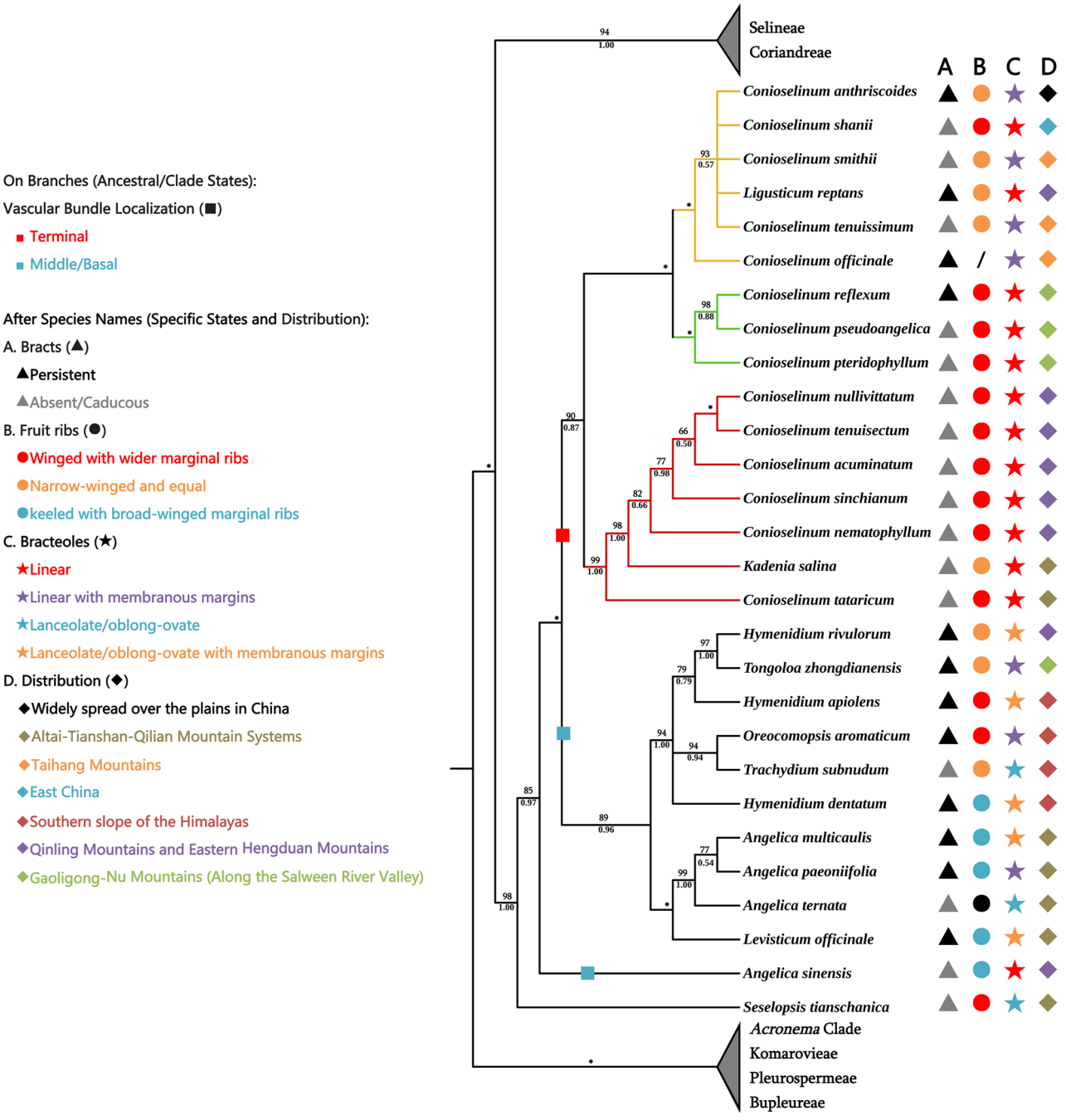

Fig. 4 The phylogenetic relationship, distribution information, morphological characteristics among Conioselinum and related groups. Symbols on branches: vascular bundle localization; Species-specific States: (**A**) Bracts: triangle; (**B**) Fruit ribs: circle; (**C**) Bracteoles: star; (**D**) Geographic Distribution: diamonds

ycf2 (protein translocation complex) may reflect adaptive modifications in RNA processing and protein import mechanisms under stressful conditions [44, 45]. Collectively, these signatures of structural dynamism and molecular selection provide pivotal insights into the evolutionary mechanisms that facilitated the successful colonization and subsequent diversification of *Conioselinum* across its ecologically disparate range.

Systematic implications and congruence between molecular and morphological traits

To address the long-standing taxonomic uncertainties outlined in our objectives, the phylogenetic analyses based on nrDNA and plastome datasets confirm that *Conioselinum* is deeply nested within the *Hymenidium* clade, rather than being polyphyletically distributed across two major clades as previously suggested [14, 15].

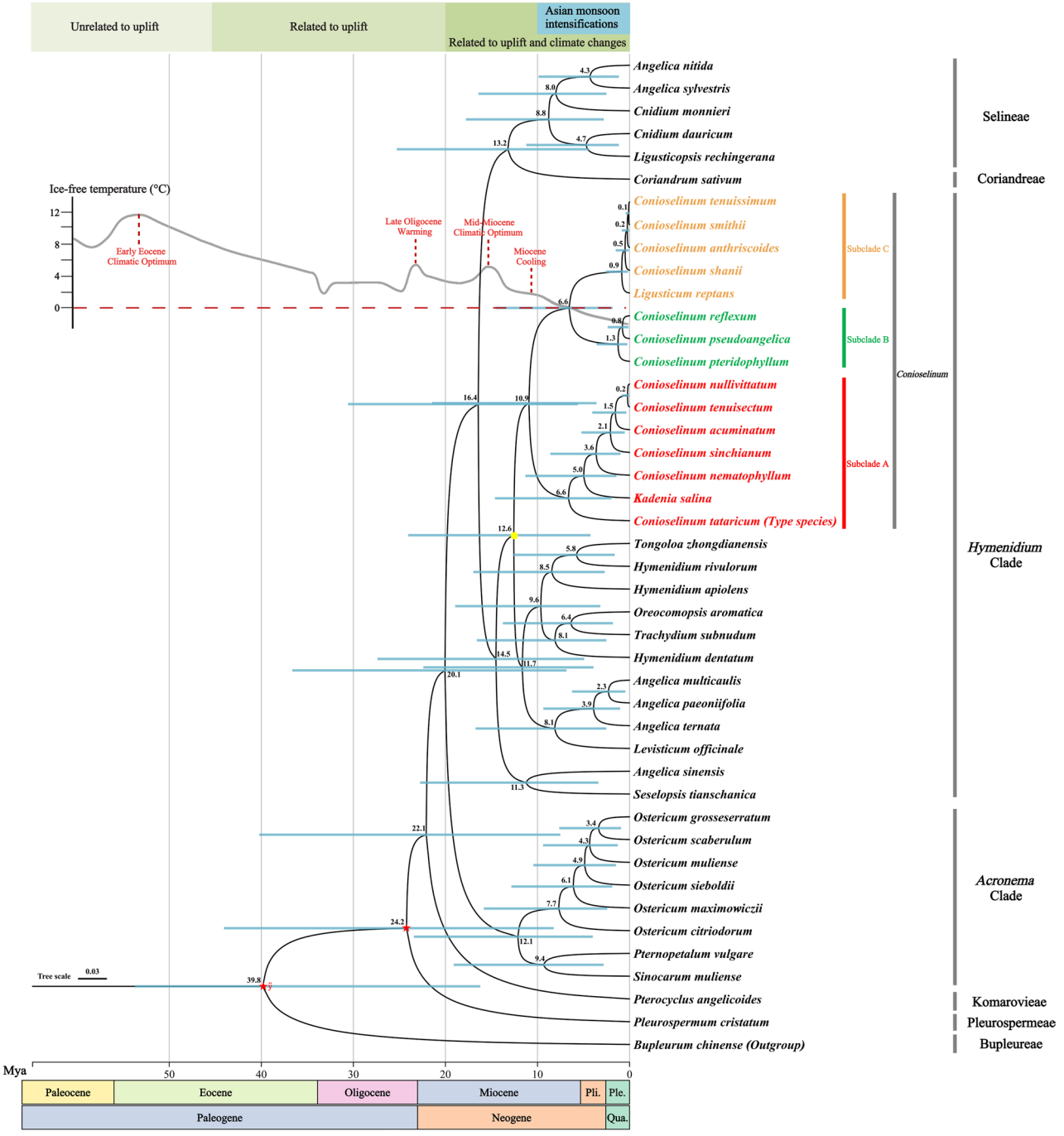

Fig. 5 The estimation of divergence times inferred from 45 nrDNA sequences and two secondary calibration points (red stars). Blue bars and numbers above represent the 95% highest posterior density (95% HPD) for each node. The scale axis is in millions of years ago (Mya). Yellow spots indicated origin nodes of *Conioselinum*. The major geological events and global temperature trend (gray curve) was modified from Favre et al. [52]

Within this framework, *Conioselinum* is shown to be closely allied with *Hymenidium*, *Levisticum*, *Seselopsis* and specific taxa from *Angelica*, *Oreocomopsis* and *Trachydium*. While both datasets support the recognition of three major subclades within the genus, we observed significant topological incongruence between the nrDNA and plastome phylogenies (Fig. 3). The plastome tree provided higher resolution for deep-level nodes but revealed relationships that conflict with the nrDNA dataset and previous classifications [5, 10, 46], suggesting a complex evolutionary history likely involving hybridization or incomplete lineage sorting.

Integrating phylogenetic analyses with morphological characteristics has led to a clearer delimitation of

Conioselinum (Fig. 4). The genus is morphologically distinguished from its allies by a specific combination of traits, most notably deciduous basal leaves, linear bracteoles, and the absence or obsolescence of calyx teeth. For phylogenetic inference, biparentally inherited nrDNA provides a more reliable framework, as its rapidly evolving non-coding regions help resolve species-level relationships. Although the bootstrap values in the plastome tree appear high (mostly 100%), this does not necessarily indicate that it represents the correct species tree. If ancient chloroplast capture events have occurred, the strong support may largely reflect the consistent evolutionary history of the chloroplast genome itself, rather than the history of species divergence. Therefore, combined analysis of morphological and nrDNA data effectively delimit *Conioselinum* from its allies using these vegetative and floral markers alongside the distal localization of vascular bundles within the fruit ribs, a stable synapomorphy that distinguishes it from related genera where vascular bundles typically reside at the rib base [4].

In light of this molecular complexity, the Subclade A—which includes the type species *C. tataricum*—emerges as the phylogenetic core of the genus. This core lineage consistently exhibits the aforementioned diagnostic suite: deciduous basal leaves, caducous or absent bracts, linear bracteoles, and obsolete calyx teeth. This anatomical marker aligns precisely with the basal divergence in our trees, reinforcing the evolutionary foundation of the genus. Across the genus, the morphological boundaries between the three subclades reflect distinct evolutionary trajectories: Subclade A taxa typically exhibit white petals and larger fruits with fewer vittae; Subclade B species share colorful petals and increased commissural vittae; and Subclade C is uniquely defined by narrow-winged fruit ribs, persistent bracts and bracteoles with narrow white membranous margins.

The case of *K. salina* (formerly *Kadenia salina*) further epitomizes the necessity of an integrative reassessment. Historically shuffled among *Cnidium* [47], *Ligusticum* [48], *Selinum* L [49]. , and *Kadenia* Lavrova & V.N.Tikhom [50], its systematic position has long been contentious. Our nrDNA phylogeny places it near the *Conioselinum* type species, whereas plastome data nests it within Subclade B. This observed cytonuclear discordance explains the historical instability in the taxonomic placement of *K. salina*. Nevertheless, its morphological characteristics—specifically the presence of linear bracteoles, obsolete calyx teeth, terminal vascular bundles, and narrowly winged fruits—clearly indicate affinity with *Conioselinum* rather than with *Cnidium* or *Kadenia* [10, 50].

The distinction between *Conioselinum* and its allies is further clarified by specific anatomical markers. *Angelica* species exhibit narrowly lanceolate bracteoles and lateral ribs that are obtuse-rounded or filiform, while *Hymenidium* taxa are distinguished by bracteoles with broad white membranous margins and a U-shaped endosperm. Despite these differences, the deciduous nature of basal leaves, linear bracteoles, absent or obsolete calyx teeth, and the terminal localization of vascular bundles remains the most diagnostic trait for *Conioselinum*. This structural evolution is deeply intertwined with the group's biogeographic history; specialized taxa in the Gaoligong–Nu Mountains and the southern Himalayas represent deep evolutionary lineages driven by topographic complexity, while northern lineages in the Altai–Tianshan–Qilian systems match the genetic variations identified in our datasets. Consequently, these findings indicate that a revised circumscription is required for *Conioselinum*. We propose that all species within the three subclades (Subclades A, B, and C) investigated in this study be included in the revised circumscription of *Conioselinum*. Future research utilizing low-copy nuclear genes will be essential to further resolve the observed cytonuclear conflicts and stabilize the taxonomy of this morphologically diverse lineage.

Divergence times and drivers of diversification

The rapid diversification of *Conioselinum* from the Late Miocene to the Pleistocene was likely orchestrated by a synergy of regional tectonic activities, global climatic oscillations, and adaptive molecular evolution. The significant discrepancy in divergence time estimations between the nrDNA and plastome datasets provides a compelling basis for a potential hybrid origin of the lineage. Our divergence time estimation indicates that the primary lineages of *Conioselinum* began to diversify during the Late Miocene (Fig. 5, marked by yellow spots), a period that coincides with the final uplift phase of the Qinghai-Tibet Plateau (QTP) uplift and the intensification of the Asian monsoon [51, 52]. These geological upheavals, alongside the progressive elevation of the Himalayas and Tianshan ranges, created complex, heterogeneous habitats and novel geographic barriers [53, 54]. We propose that the colonization of these emerging high-altitude niches served as a powerful selective force, as evidenced by the positive selection identified in the *ycf1* gene (see 3.1). This molecular signature of adaptation likely bolstered the resilience of *Conioselinum* ancestors to alpine abiotic stressors, such as elevated UV radiation and extreme temperature fluctuations, thereby facilitating the initial divergence of Subclades A and C into these newfound ecological spaces [55].

The evolutionary trajectory of *Conioselinum* further intensified during the late Quaternary, particularly within the Hengduan Mountains to Gaoligong Mountains region. The three species comprising Subclade B (*C. reflexum*, *C. pseudoangelica*, and *C. pteridophyllum*) are

narrow endemics of this region. The intense uplift of the Hengduan Mountains and the subsequent incisement of deep river valleys (Yangtze, Mekong, and Salween) provided the requisite geographic isolation for such montane diversification [51, 56–59]. Concurrently, the relaxed purifying selection observed in genes like *rpoA*, *rps7*, and *ccsA* suggests a fine-tuning of chloroplast transcription and translation, reflecting adaptive functional shifts as these lineages occupied specialized micro-habitats within the "sky island" archipelago [60–62].

However, the evolutionary history of the genus is not solely a product of isolation but also of reticulate evolution. The significant cytonuclear discordance observed between our nrDNA and plastome phylogenies points toward a complex interplay of hybridization, introgression, and incomplete lineage sorting (ILS) [28, 29, 33]. There are prior reports of hybridization within *Conioselinum* revealed that the medicinal cultivar *C. anthriscoides 'Chuanxiong'* likely originated through hybridization involving wild *C. anthriscoides* populations and an unidentified maternal donor [63, 64]. The propensity for hybridization is particularly evident in Subclade C, where recent speciation may still be ongoing. This is further corroborated by the polyploid nature of *C. pteridophyllum* (4n = 44), whose double chromosome count distinguishes it from the diploid congeners (2n = 22) [23]. Furthermore, the sympatry of *Conioselinum* with related genera such as *Tongoloa* H. Wolff, *Selinum*, and *Ligusticum* in alpine regions heightens the possibility of chloroplast capture [65–67], a phenomenon that likely obscured the phylogenetic relationships within the plastome framework. According to the molecular dating, the stem of *Conioselinum* originated in the Late Miocene, with the nrDNA-based estimate of approximately 12.58 Ma (95% HPD: 4.25–24.05 Ma) being notably older than the plastome-based estimate of 6.84 Ma (95% HPD: 1.72–15.75 Ma). This temporal asymmetry suggests a historical "chloroplast capture" event following ancestral hybridization; specifically, the common ancestor of the *Conioselinum* complex likely acquired a new maternal genome through hybridization with a related lineage during the Late Miocene, followed by rapid radiation driven by intensifying geological activity. This hypothesis is further supported by the remarkably recent and clustered plastome divergence times for Subclades B and C (3.75–7.18 Mya) base on plastomes, which indicate that these lineages may have emerged from a series of frequent gene flow exchanges or reticulate evolution events during the Pliocene. Collectively, the combination of tectonic-driven isolation, molecular adaptation to alpine stress, and hybridization events explains both the rapid radiation of *Conioselinum* and the taxonomically challenging nature of this morphologically diverse complex.

Conclusion

Integrating genome skimming with carpological evidence, this study establishes a robust phylogenetic framework for the genus *Conioselinum*. The nrDNA-based phylogeny confirms that *Conioselinum* is a monophyletic lineage nested within the *Hymenidium* clade and comprises three primary subclades (A, B, and C). This phylogenetic structure shows strong concordance with a distinct suite of macro-morphological characters, specifically deciduous basal leaves, linear bracteoles, and absent or obsolete calyx teeth. Crucially, this research reaffirms that the terminal localization of vascular bundles in fruit ribs constitutes a stable synapomorphy for *Conioselinum* when integrated with these vegetative and floral markers, providing a definitive anatomical marker to distinguish it from closely related allies. Combining phylogenetic and morphological evidence, we propose a revised circumscription of *Conioselinum* to include all species comprising these three subclades.

The observed topological incongruence between the plastome and nuclear phylogenies reflects a complex evolutionary history likely shaped by ancient chloroplast capture or hybridization. Despite these cytonuclear conflicts, the integration of phylogenomic and carpological data provides a solid foundation for the formal taxonomic revision of the genus. Future studies employing population-level sampling and low-copy nuclear genes will be essential to further resolve these evolutionary complexities and refine species-level boundaries within this morphologically diverse lineage.

Materials and methods

Taxon sampling, DNA extraction and sequencing

Fresh leaf samples representing 22 taxa—including 14 *Conioselinum* species and eight closely related taxa (one *Ligusticum* species, three *Cnidium* species, two *Angelica* species, and one species each from *Levisticum* and *Seselopsis*)—were collected during field surveys. verified by comparing morphological characters with type specimens, relevant taxonomic literature, and authenticated herbarium specimens. Formal identification was performed by Meng-Die Liu and Professor Song-Dong Zhou (Sichuan University). All voucher specimens were deposited in the Herbarium of Sichuan University (CDBI), Chengdu, China (Table S1).

Total genomic DNA was extracted from silica gel-dried leaf tissues using a modified cetyltrimethylammonium bromide (CTAB) protocol [68]. To obtain high-density genomic resources, whole-genome skimming was conducted on the Illumina NovaSeq platform (Personalbio, Shanghai, China). The sequencing generated 150-bp paired-end reads, yielding approximately 10 Gb of raw data per sample, ensuring sufficient coverage for the assembly of complete plastomes and nrDNA clusters.

Genome assembly and comparative genomics

Raw sequencing data were processed using AdapterRemoval v2 [69] and fastP v0.15.0 [70] to generate high-quality clean reads (Q30 > 90%). For each sample, plastomes and nrDNA sequences were assembled *de novo* using NOVOPlasty [71]. Plastomes were annotated with Plastid Genome Annotator (PGA) and manually proofread in Geneious Prime v2025.0.2 [72, 73]. Final plastome annotations were visualized using Organellar Genome DRAW (OGDRAW) [74]. The nrDNA sequences were delimited by mapping to reference sequences (*Musa coccinea*, GenBank accession LC610755) and identifying conserved ribosomal motifs [75–77]. All newly obtained sequences (Table S7) were uploaded to GenBank.

To evaluate genomic divergence, comparative analyses were performed across 16 representative taxa (14 *Conioselinum* species and two close biological allies). IRscope was employed to analyze the boundaries between inverted repeat (IR) and single copy (SC) regions [78]. The nucleotide diversity (Pi), nonsynonymous (Ka) and synonymous (Ks) nucleotide substitution rates were calculated using DnaSP v6.12.03 [79]. Additionally, genomic conservation was evaluated with mVISTA's Shuffle-LAGAN alignment algorithm [74] and Mauve Alignment [80] plugin in Geneious Prime, employing *Conioselinum tataricum* as the reference. Protein-coding genes (CDS) longer than 300 bp were extracted for subsequent adaptive evolution analyses [81, 82]. Relative synonymous codon usage (RSCU) values were calculated using CodonW [83] and RSCU values were visualized as heatmaps in TBtools [84].

Phylogenetic analysis

To resolve the phylogenetic position of *Conioselinum*, two datasets derived from 45 taxa were analyzed. The first, a nrDNA dataset spanning 5,833 bp (comprising 30 newly generated sequences), included partial ETS, 18 S, ITS1, 5.8 S, ITS2, and partial 26 S regions. This dataset exhibited a high level of sequence variation, with 600 (10.29%) variable sites and 355 (6.09%) parsimony-informative sites (PIS). Compared with the standard ITS region (620 bp), the nrDNA alignment provided a substantial increase in the total number of informative characters. The second, a plastid protein-coding gene (PCG) dataset, encompassed 66,589 bp (comprising 22 newly sequences) across 79 protein-coding genes. Despite its lower overall percentage of variation compared to the nrDNA data, the plastome dataset yielded a vastly greater absolute number of informative sites, featuring 5,487 (8.24%) variable sites and 1,908 (2.87%) PIS. Based on previous phylogenetic analyses [15, 37], *Bupleurum chinense* Franch. was selected as the outgroup, given its early-diverging position within the subfamily *Apioideae*.

Phylogenetic reconstruction was performed using Maximum Likelihood (ML) and Bayesian Inference (BI). For the nrDNA dataset, a partitioned strategy was applied to separate conserved ribosomal subunits from variable spacers, with best-fit models selected via ModelFinder [85] under the Bayesian Information Criterion (BIC). ML trees were reconstructed using IQ-TREE v2.4.0 [82, 86] with 1,000 ultrafast bootstrap replicates. For the plastid dataset, concatenated ML analysis was performed using RAxML v8.2.10 [87] (GTRGAMMA model), and a coalescent-based species tree was estimated using ASTRAL v5.7.1 [88] based on 79 individual gene trees generated by IQ-TREE.

For BI analysis of both datasets, MrBayes v3.2.7 [89] was employed with two independent runs and four MCMC chains for 2,000,000 generations (sampling every 100 generations). The first 25% of samples were discarded as burn-in. MCMC convergence and stationarity were confirmed by: (i) ASDSF < 0.01; (ii) PSRF = 1.000 for all parameters; and (iii) ESS > 200 as verified in Tracer v1.7.2 [90]. All trees were visualized using iTOL v6 [91].

Morphological and anatomical observations

To evaluate the phenotypic divergence and identify diagnostic characters within *Conioselinum* and related genera, morphological characteristics (including whole plants, flowers, and roots) were observed in their natural habitats (Table S4 and S5). Fully mature fruits from 20 taxa (Table S8) were preserved in formaldehyde-acetic acid-ethanol (FAA) solution. Samples from 16 taxa were examined and photographed using a Nikon stereomicroscope (Tokyo, Japan), with 10 mericarps measured per species to assess carpological variation (Fig. 3). For anatomical analysis to compare fruit internal structures that may reflect phylogenetic relationships, mature mericarps from 16 taxa were processed for paraffin sectioning according to the following protocol (Figure S6): tissues fixed in FAA were dehydrated through an ethanol series, cleared in xylene, and embedded in paraffin; serial sections were cut using a rotary microtome, stained with safranin-fast green, and finally mounted for bright-field microscopy observation. Additional morphological data were cross-referenced with type specimens, *Flora of China* [10, 46], and previous literature [4, 92] to ensure accurate species identification and trait comparison.

Molecular dating

Divergence times were estimated using MCMCTree of PAML v4.10.7 [93] based on two molecular datasets: nrDNA and plastome 79 CDS (Table S6). Due to the scarcity of reliable macrofossils in Apiaceae, we utilized two secondary calibration points anchored by the family's most definitive microfossil records (pollen) as reassessed [94]: (i) the stem node of Bupleureae, constrained

by Priabonian pollen fossils with a minimum age of 33.90 Mya; and (ii) the stem node of Pleurospermeae, similarly constrained by Priabonian fossil records. These calibration points were implemented with a normal distribution prior, using mean ages and standard deviations derived from the 95% HPD intervals (39.49–52.41 Mya and 36.65–47.8 Mya, respectively).

The MCMC analysis was performed with the following parameters: 5×10^8 generations, with trees sampled every 2,000 generations, and the first 25% of samples discarded as burn-in. To ensure the reliability of the time estimates, convergence was verified using Tracer v1.7.2 [90], confirming that the effective sample size (ESS) for all parameters was ≥ 200, indicating sufficient sampling and stationarity of the MCMC chains. The final consensus tree was viewed in FigTree [95] and tvBOT v2.6.1 [96], displaying node ages and 95% highest posterior density intervals (95% HPDs) for divergence times.

Supplementary Information

The online version contains supplementary material available at https://doi.org/10.1186/s12870-026-08347-7.

Supplementary Material 1. Figure S1. Comparison of LSC, SSC and IR boundary regions for sixteen plastomes. JLA: junction of LSC/IRa. JLB: junction of LSC/IRb. JSA: junction of SSC/IRa. JSB: junction of SSC/IRb.

Supplementary Material 2. Figure S2. The RSCU values of 53 protein-coding regions for sixteen plastomes. Red represents higher RSCU values, while blue indicates lower RSCU values.

Supplementary Material 3. Figure S3. Sequence identity plots for sixteen plastomes. Reference plastome: *C. tataricum*.

Supplementary Material 4. Figure S4. Mauve alignment of sixteen plastomes, purple boxes highlight the gene gains.

Supplementary Material 5. Figure S5. Species tree of *Conioselinum* and allied genera inferred from ASTRAL-III analysis based on 79 plastid coding sequences. Numbers at the nodes indicate local posterior probability (LPP) values. Three primary subclades A (Red), B (Green), and C (Yellow) are recovered with high support.

Supplementary Material 6. Figure S6. Mericarp anatomy of 16 taxa, *Conioselinum* (A—M) and closely related genera (N—P), Scale bars = 1 mm. (A) *Conioselinum tataricum*; (B) *C. nematophyllum*; (C) *C. acuminatum*; (D) *C. tenuisectum*; (E) *Liguticum reptans*; (F) *C. smithii*; (G) *C. tenuissimum*; (H) *C. anthriscoides*; (I) *C. shanii*; (J) *C. pseudoangelica*; (K) *C. pteridophyllum*; (L) *C. reflexum*; (M) *Kadenia salina*; (N) *Oreocomopsis aromatica*; (O) *Hymenidium apiolens*; (P) *Angelica multicaulis*; vascular bundles (VB); endosperm (ES); dorsal ribs (DR), lateral ribs (LR), marginal ribs (MR); parenchyma cells with lignified pitted walls (PP), furrow vittae (VV), and the commissure vittae (CV); Scale bars =1 mm.

Supplementary Material 7. Figure S7. Assessing nucleotide diversity (Pi) across sixteen plastomes through comparative analysis: (a) 53 protein-coding genes, (b) 65 intergenic regions.

Supplementary Material 8. Figure S8. Average nonsynonymous (Ka) (a), synonymous (Ks) (b), and Ka/Ks (c) values of 53 protein-coding genes from sixteen plastomes.

Supplementary Material 9. Table S1. Voucher information for newly sequenced species in this study, including collection locality, herbarium voucher details.

Supplementary Material 10. Table S2. List of unique genes identified in plastomes of *Conioselinum*.

Supplementary Material 11. Table S3. Codon usage and relative synonymous codon usage (RSCU) values of protein-coding genes of the sixteen *Conioselinum* plastomes.

Supplementary Material 12. Table S4. Comparison of morphological characters (fruit part) of *Conioselinum* and related taxa in this study, data from description of personal observations, Flora of China and related researches.

Supplementary Material 13. Table S5. Comparison of morphological characters (vegetative and flower part) of *Conioselinum* and related taxa in this study, data from description of personal observations, Flora of China and related researches.

Supplementary Material 14. Table S6. Comparative analysis of alignment characteristics and estimated divergence times for major Apiaceae clades based on different molecular datasets.

Supplementary Material 15. Table S7. nrDNA and plastomes included in phylogenetic analyses with GenBank accession. Newly sequenced sequences are bold.

Supplementary Material 16. Table S8. Sources of fruits of *Conioselinum* and allied genera.

Acknowledgements
We are grateful to Qiu-Ping Jiang, Li-Jia Liu, An-Qi Zhao and Xue-Li Huang for their help in samples collection. We are grateful to the herbarium curators for providing information on the type specimens and the help they gave us in searching for type materials.

Authors' contributions
MD: Investigation, Methodology, Data curation, Writing (original draft), Formalanalysis. ZX: Investigation, Methodology, Data curation. WY: Investigation, Data curation. TR: Investigation. BN: Methodology, Software. XJ, DF, and SD: Supervision, Methodology, Data curation, Writing (review & editing). All authors read and approved the final manuscript.

Funding
This work was supported by the National Natural Science Foundation of China (Grant Nos. 32470216, 32170209). The funders were not involved in the design of the study, collection, analysis and interpretation of data, and manuscript preparation.

Data availability
The nrDNA sequences (accession numbers: PV609723–PV609761) and annotated plastomes (accession numbers: PV613211–PV613240) are publicly accessible via the NCBI database (https://www.ncbi.nlm.nih.gov); detailed accession numbers are listed in Table S7.

Declarations

Ethics approval and consent to participate
All samples collected fully adhere to national and local legal requirements. The plant samples used in the study were neither listed as nationally protected nor gathered from national parks or natural reserves. No specific permissions were necessary for their collection according to national and local laws.

Consent for publication
Not applicable.

Competing interests
The authors declare no competing interests.

Received: 29 September 2025 / Accepted: 6 February 2026
Published online: 13 February 2026

References

1. Hoffmann GF. Genera Plantarum Umbelliferarum Eorumque Characteres Naturales Secundum Numerum, Figuram, Situm Et Proportionem Omnium

Fructificationis Partium: Accedunt Icones Et Analyses æri Incisæ. Mosquæ: sumtibus auctoris, typis N.S. Vsevolozskianis; 1814-16:180-185.
2. Mathias ME, Constance L. North American flora, vol. v. 28B. Volume 45. New York: New York Botanical Garden; 1944.
3. Bulletin K. Index Kewensis: on compact disc. 1997.
4. Pimenov M, Kljuykov E, Ostroumova T. A revision of Conioselinum Hoffm. (Umbelliferae) in the Old World. Willdenowia 2003;33(2):353-77.
5. Pimenov M. Updated checklist of Chinese Umbelliferae: nomenclature, synonymy, typification, Distribution. In: 2017.
6. Torrey J, Gray A. A flora of North america:containing abridged descriptions of all the known Indigenous and naturalized plants growing North of Mexico, arranged according to the natural system. Volume 1. New York: Wiley & Putnam; 1838. pp. 1838–40.
7. Hermann F. Flora of northern and central Europe. In: 1956.
8. Musselman LJ. The vegetation of Mongolia. Econ Bot. 2008;51:89.
9. Wu Z, Raven PH, Missouri Botanical G. Flora of China. Beijing: St. Louis:: Beijing : Science Press;; 1994.
10. Pan ZH, Watson MF. Flora of China. Beijing: Science; 2005.
11. Sinicae B-OA. Flora Tsinlingensis. 1981;1(3):415-17.
12. Kondo K, Terabayashi S, Okada M, Yuan C, He S. Phylogenetic relationship of medicinally important Cnidium officinale and Japanese apiaceae based on RbcL sequences. J Plant Res. 1996;109(1):21–7.
13. Downie SR, Katz-Downie DS, Watson MF. A phylogeny of the flowering plant family apiaceae based on Chloroplast DNA rpl16 and rpoC1 intron sequences: towards a suprageneric classification of subfamily Apioideae. Am J Bot. 2000;87(2):273–92.
14. Downie SR, Spalik K, Katz-Downie DS, Reduron JP. Major clades within apiaceae subfamily Apioideae as inferred by phylogenetic analysis of NrDNA ITS sequences. Plant Divers Evol. 2010;128:111–36.
15. Zhou J, Gao YZ, Wei J, Liu ZW, Downie SR. Molecular phylogenetics of ligusticum (Apiaceae) based on NrDNA ITS sequences: rampant Polyphyly, placement of the Chinese endemic Species, and a Much-Reduced circumscription of the genus. Int J Plant Sci. 2020;181:306–23.
16. Shu PaS ML. Zhongguo Sanxingke Zhiwu Huafen Tuzhi [Pollen atlas of Chinese umbelliferous Plants]. Shanghai: Shanghai Scientific and Technical; 2001.
17. Tellería MC, Daners G. Pollen types in Southern new world convolvulaceae and their taxonomic significance. Plant Syst Evol. 2003;243(1):99–118.
18. Wang P. Pollen morphology and its relationship of ligusticum Sinense cv.Chuanxiong, L. Sinense cv.Fuxiong and L. Sinense. Acta Bot Yunnanica. 1990;12(2):173–8.
19. Zhou J, Liu Z-W. Comparative morphology of the leaf epidermis in ligusticum (Apiaceae) from China. Am J Plant Sci. 2018;09:1105–23.
20. Ostroumova T, Kljuykov E. Stomatal types in Chinese and Himalayan umbelliferae. Feddes Repertorium. 2007;118:84–102.
21. Volkova S. The leaf epidermis of Conioselinum longifolium and C. tataricum (Apiaceae, Ligusticeae), growing in Siberia. Turczaninowia. 2016;19:19–26.
22. Zhang H-D. Studies on the origin of the traditional Chinese drug Jinxiong. J Univ Chin Acad Sci. 1990;28(6):6.
23. Zhou J, Pu FD, Peng H, Pan YZ, Gong X. Karyological studies of ten ligusticum species (Apiaceae) from the Hengduan mountains region of China. Caryologia. 2008;61(4):333–41.
24. Gui LJ, Xie DF, Ren T, Yu LY, He XJ. Chloroplast genomes and ribosomal DNA provide insights into divergence and morphological evolution of alpine Tongoloa. J System Evol. 2023;63:72-84.
25. Lv S, Ye X, Li Z, Ma P, Li D. Testing complete plastomes and nuclear ribosomal DNA sequences for species identification in a taxonomically difficult bamboo genus fargesia. Plant Divers. 2023;45:147–55.
26. Guo X-L, Gou W, Peng C, He X-J. New insights into the phylogenetic position of hymenidium dentatum (Apioideae, Apiaceae) inferred from NrDNA and morphological evidence. Phytotaxa. 2020;452:46–54.
27. Zhang T, Fang Y, Wang X, Deng X, Zhang X, Hu S, Yu J. The complete Chloroplast and mitochondrial genome sequences of Boea hygrometrica: insights into the evolution of plant organellar genomes. PLoS ONE. 2012;7(1):e30531.
28. Spooner D, Ruess H, Ellison S, Senalik D, Simon P. What is truth: consensus and discordance in next-generation phylogenetic analyses of Daucus. J Syst Evol. 2020;58(6):1059-70.
29. Dong S-S, Wang Y-L, Xia N-H, Liu Y, Liu M, Lian L, Li N, Li L-F, Lang X-A, Gong Y-Q, et al. Plastid and nuclear phylogenomic incongruences and biogeographic implications of Magnolia s.l.(Magnoliaceae). J Syst Evol. 2022;60(1):1–15.
30. Stern DL. The genetic causes of convergent evolution. Nat Rev Genet. 2013;14(11):751–64.
31. Li H-T, Yi T-S, Gao L-M, Ma P-F, Zhang T, Yang J-B, Gitzendanner MA, Fritsch PW, Cai J, Luo Y, et al. Origin of angiosperms and the puzzle of the jurassic gap. Nat Plants. 2019;5(5):461–70.
32. Fu C-N, Mo Z-Q, Yang J-B, Cai J, Ye L-J, Zou J-Y, Qin H-T, Zheng W, Hollingsworth PM, Li D-Z, et al. Testing genome skimming for species discrimination in the large and taxonomically difficult genus rhododendron. Mol Ecol Resour. 2022;22(1):404–14.
33. Yang YZ, Sun PC, Lv LK, Wang DL, Xi ZX, Wang XY, Davis CC, Liu JQ. Prickly waterlily and rigid hornwort genomes shed light on early angiosperm evolution. Nat Plants. 2020;6(3):215–22.
34. Li ZX, Guo XL, Price M, He XJ. Phylogenetic position of Ligusticopsis (Apiaceae, Apioideae): evidence from molecular data and carpological characters. AoB PLANTS 2022, 14.
35. Liu C, Lei J, Jiang Q-P, He X-J. The complete plastomes of seven peucedanum plants: comparative and phylogenetic analyses for the peucedanum genus. BMC Plant Biol. 2022;22(1):101.
36. Ren T, Xie D, Peng C, Gui L, Price M, Zhou S, He X. Molecular evolution and phylogenetic relationships of ligusticum (Apiaceae) inferred from the whole plastome sequences. BMC Ecol Evol. 2022;22(1):55.
37. Wen J, Xie DF, Price M, Ren T, Deng YQ, Gui LJ, Guo XL, He XJ. Backbone phylogeny and evolution of Apioideae (Apiaceae): new insights from phylogenomic analyses of plastome data. Mol Phylogenet Evol. 2021;161:107183.
38. Hansen D, Dastidar S, Cai Z, Penaflor C, Kuehl J, Boore J, Jansen R. Phylogenetic and evolutionary implications of complete Chloroplast genome sequences of four early-diverging angiosperms: buxus (Buxaceae), Chloranthus (Chloranthaceae), Dioscorea (Dioscoreaceae), and illicium. Mol Phylogenet Evol. 2007;45:547–63.
39. Huang H, Shi C, Liu Y, Mao SY, Gao LZ. Thirteen camellia Chloroplast genome sequences determined by high-throughput sequencing: genome structure and phylogenetic relationships. BMC Evol Biol. 2014;14:151.
40. Drescher A, Ruf S Jr, Carrer T, Bock H. The two largest Chloroplast genome-encoded reading frames of higher plants are essential genes. Plant J. 2000;22:97–104.
41. Schmid L-M, Manavski N, Chi W, Meurer J. Chloroplast ribosome biogenesis factors. Plant Cell Physiol. 2023;65(4):516-536.
42. Fakih Z, Plourde B, Germain M. H: Differential Participation of Plant Ribosomal Proteins from the Small Ribosomal Subunit in Protein Translation under Stress. Biomolecules. 2023;13(7):1160.
43. Kindgren P, Strand A. Chloroplast transcription, untangling the gordian knot. New Phytol. 2015;206:889–91.
44. Xie ZY, Merchant S. The Plastid-encoded CcsA gene is required for Heme attachment to Chloroplast c-type cytochromes. J Biol Chem. 1996;271:4632–9.
45. Zhang Z-R, Yang X, Li W-Y, Peng Y-Q, Gao J. Comparative Chloroplast genome analysis of ficus (Moraceae): insight into adaptive evolution and mutational hotspot regions. Front Plant Sci. 2022;13:965335.
46. Shan RH. I. SM: In: Conioselinum Fisch. ex Hoffm. In Flora Republicae Popularis Sinicae. Edited by Shan R-h, Sheh M-l. 1985, vol. 55(3):p2-4.
47. Moskovskoe obshchestvo liubitelei p. Bulletin de La Société impériale des Naturalistes de Moscou, vol. t.17:no.1–4 (1844). Moscou: Société impériale des naturalistes de Moscou; 1844.
48. Moskovskoe obshchestvo liubitelei p. Bulletin de La Société impériale des Naturalistes de Moscou, vol. New ser.:t.29–30 (1915–1916). Moscou: Société impériale des naturalistes de Moscou; 1915.
49. Busik VV, Malyshev LI, Peshkova GA. Sibirskiĭ Institut Fiziologii i Biokhimii r, T♫S↯entral'nyĭ sibirskiĭ botanicheskiĭ s: Флора Центральной Сибири. Изд-во Наука, Сибирское отд-ние; 1979.
50. Moskovskoe obshchestvo liubitelei p. Byulleten' Moskovskogo obshchestva ispytatelei Prirody. Otdel biologicheskii. Volume 91. Moscou: Société impériale des naturalistes de Moscou; 1986. p. 93. 2.
51. Mulch A, Chamberlain C. Earth science: the rise and growth of Tibet. Nature. 2006;439:670–1.
52. Favre A, Päckert M, Pauls S, Jähnig S, Uhl D, Michalak I, Muellner-Riehl A. The role of the uplift of the Qinghai-Tibetan plateau for the evolution of Tibetan biotas. Biol Rev. 2015;90:236–53.
53. Ding L, Kapp P, Cai F, Garzione C, Xiong Z, Wang H, Wang C. Timing and mechanisms of Tibetan plateau uplift. Nat Reviews Earth Environ. 2022;3:1–16.
54. Mao K, Wang Y, Liu J. Evolutionary origin of species diversity on the Qinghai-Tibet plateau. J Syst Evol. 2021;59(6):1142-1158.
55. Guo Z, Peng S, Hao Q, Biscaye PE, Liu TS. Origin of the Miocene–Pliocene Red-Earth formation at Xifeng in Northern China and implications for

paleoenvironments. Palaeogeography Palaeoclimatology Palaeoecology. 2001;170:11–26.
56. Li J, Fang X. Uplift of Tibetan plateau and environmental changes. Chin Sci Bull. 1999;44:2117–24.
57. Zheng H, Powell C, An Z, Zhou J, Dong G. Pliocene uplift of the Northern Tibetan Plateau. Geology. 2000;28(8):715–718.
58. Sun B, Wu J-Y, Ding S-T, Xiangchuan L, Xie S, Yan D-F, Lin Z-C. Reconstructing neogene vegetation and climates to infer tectonic uplift in Western Yunnan, China. Palaeogeography Palaeoclimatology Palaeoecology - PALAEOGEOGR PALAEOCLIMATOL. 2011;304:328–36.
59. Zhang J-Q, Shiyong M, Allen G, Wen J, Rao G-Y. Rapid radiation and dispersal out of the Qinghai-Tibetan plateau of an alpine plant lineage Rhodiola (Crassulaceae). Mol Phylogenet Evol. 2014;77:147-58.
60. He K, Jiang X-L. Sky Islands of Southwest China. I: an overview of phylogeographic patterns. Chin Sci Bull. 2014;59:1–13.
61. Chen J-H, Huang Y, Brachi B, Yun Q-z, Zhang W, Lu W, Li W-q, Sun X, Wang G, He J et al. Genome-wide analysis of cushion Willow provides insights into alpine plant divergence in a biodiversity hotspot. Nat Commun. 2019;10(1):5230.
62. Zhang D, Hao GQ, Guo X, Hu QJ, Liu J. Genomic insight into the 'Sky islands' species diversification in a mountainous biodiversity hotspot. J Syst Evol. 2019;57(6):633-645.
63. Nie B, Chen X, Hou Z, Guo M, Li C, Sun W, Ji J, Zang L, Yang S, Fan P, et al. Haplotype-phased genome unveils the butylphthalide biosynthesis and homoploid hybrid origin of ligusticum Chuanxiong. Sci Adv. 2024;10:eadj6547.
64. Lee S-H, Choi H-W, Sung J-S, Bang J-W. Inter-genomic relationships among three medicinal herbs: Cnidium officinale, ligusticum Chuanxiong and Angelica polymorpha. Genes Genomics. 2010;32:95–101.
65. Piwczyński M, Dinka M, Trzeciak P, Walczak K, Puchałka R, Soghigian J, Spalik K. Conflicting phylogenetic signals obscure the taxonomic position of ferula heuffelii (Apiaceae), a rare Southeast European endemic. Botanical Journal of the Linnean Society; 2025.
66. Calviño C, Martínez S, Downie S. The evolutionary history of eryngium (Apiaceae, Saniculoideae): rapid radiations, long distance dispersals, and hybridizations. Mol Phylogenet Evol. 2008;46:1129–50.
67. Jia Y, Liu M, López-Pujol J, Jia R-W, Kou Y-X, Yue M, Guan T-X, Li Z. The hybridization origin of the Chinese endemic herb genus notopterygium (Apiaceae): evidence from population genomics and ecological niche analysis. Mol Phylogenet Evol. 2023;182:107736.
68. Pahlich E, Gerlitz C. A rapid DNA isolation procedure for small quantities of fresh leaf tissue. Phytochemistry. 1980;19:11–3.
69. Davis JI, McNeal JR, Barrett CF. Contrasting patterns of support among plastid genes and genomes for major clades of the monocotyledons. Early Events Monocot Evol. 2013;Systematics Association Special Volume Series:315–49.
70. Chen SZY, Chen Y, Gu J. fastp: an ultra-fast all-in-one FASTQ preprocessor. Bioinformatics (Oxford, England) 2018;34(17):i884-i890.
71. Dierckxsens N, Mardulyn P, Smits G. NOVOPlasty: de Novo assembly of organelle genomes from whole genome data. Nucleic Acids Res. 2016. https://doi.org/10.1093/nar/gkw955.
72. Qu XJ, Moore M, Li DZ, Yi TS. PGA: A software package for rapid, accurate, and flexible batch annotation of plastomes. Plant Methods. 2019;15:1–12.
73. Kearse M, Moir R, Wilson A, Stones-Havas S, Cheung M, Sturrock S, Buxton S, Cooper A, Markowitz S, Duran C, et al. Geneious basic: an integrated and extendable desktop software platform for the organization and analysis of sequence data. Bioinf (Oxford England). 2012;28:1647–9.
74. Greiner S, Lehwark P, Bock R. OrganellarGenomeDRAW (OGDRAW) version 1.3.1: expanded toolkit for the graphical visualization of organellar genomes. Nucleic Acids Res. 2019;47:W59–64.
75. Baldwin BG. Phylogenetic utility of the internal transcribed spacers of nuclear ribosomal DNA in plants: an example from the compositae. Mol Phylogenet Evol. 1992;1(1):3–16.
76. Downie S, Katz-Downie D. A molecular phylogeny of apiaceae subfamily apioideae: evidence from nuclear ribosomal DNA internal transcribed spacer sequences. Am J Bot - Amer J Bot. 1996;83(2):234-251.
77. Downie S, Ramanath S, Katz-Downie D, Llanas E. Molecular systematics of apiaceae subfamily apioideae: phylogenetic analyses of nuclear ribosomal DNA internal transcribed spacer and plastid RPO C1 intron sequences. Am J Bot. 1998;85(4):563.
78. Amiryousefi A, Hyvönen J, Poczai P. IRscope: an online program to visualize the junction sites of Chloroplast genomes. Bioinf (Oxford England). 2018;34(17):3030-3031.
79. Librado PJR, Rozas J. DnaSP v5: A software for comprehensive analysis of DNA polymorphism data. Bioinf (Oxford England). 2009;25:1451–2.
80. Darling A, Mau B, Perna N. ProgressiveMauve: multiple genome alignment with gene gain, loss and rearrangement. PLoS ONE. 2010;5:e11147.
81. Katoh K, Standley D, Katoh K, Standley DM. MAFFT multiple sequence alignment software version 7: improvements in performance and usability. Mol Biol Evol. 2013;30(4):772-80.
82. Zhang D, Gao FL, Li WX, Jakovlić I, Zou H, Zhang J, Wang G. PhyloSuite: an integrated and scalable desktop platform for streamlined molecular sequence data management and evolutionary phylogenetics studies; 2018.
83. Peden J. Analysis of codon usage. 1999.
84. Chen CJ, Chen H, Zhang Y, Thomas H, Frank M, He YH, Xia R. TBtools - an integrative toolkit developed for interactive analyses of big biological data; 2020.
85. Kalyaanamoorthy S, Minh B, Wong T, von Haeseler A, Jermiin L. ModelFinder: fast model selection for accurate phylogenetic estimates. Nat Methods. 2017;14(6):587-589.
86. Nguyen L-T, Schmidt HA, von Haeseler A, Minh BQ. IQ-TREE: A fast and effective stochastic algorithm for estimating Maximum-Likelihood phylogenies. Mol Biol Evol. 2015;32(1):268–74.
87. Stamatakis A. RAxML version 8: A tool for phylogenetic analysis and Post-Analysis of large phylogenies. Bioinf (Oxford England). 2014;30(9):1312-3.
88. Zhang C, Rabiee M, Sayyari E, Mirarab S. ASTRAL-III: polynomial time species tree reconstruction from partially resolved gene trees. BMC Bioinformatics. 2018;19(6):153.
89. Ronquist F, Teslenko M, Mark P, Ayres D, Darling A, Höhna S, Larget B, Liu L, Suchard M, Huelsenbeck J. MrBayes 3.2: efficient bayesian phylogenetic inference and model choice across a large model space. Syst Biol. 2012;61:539–42.
90. Rambaut A, Drummond A, Xie D, Baele G, Suchard M. Posterior Summarization in Bayesian Phylogenetics Using Tracer 1.7. Systematic biology. 2018;67(5):901-904.
91. Letunic I, Bork P. Interactive Tree Of Life (iTOL) v4: recent updates and new developments. Nucleic acids research 2019, 47:W256-W259.
92. Ren T, Gui LJ, Wen J, Song BN, Peng C, Xie DF, Zhou SD, He XJ. Taxonomy of the Chinese ligusticum s. l. revisited by molecular data and mericarp morphology. Bot J Linn Soc. 2025;209(4):331–344.
93. Yang ZH. PAML 4: Phylogenetic analysis by maximum likelihood. Mol Biol Evol 24: 1586–1591. Molecular biology and evolution. 2007;24:1586–1591.
94. Wen J, Yu Y, Xie DF, Peng C, Liu Q, Zhou SD, He XJ. A transcriptome-based study on the phylogeny and evolution of the taxonomically controversial subfamily Apioideae (Apiaceae). Ann Botany. 2020;125(6):937–53.
95. Rambaut A. FigTree, a graphical viewer of phylogenetic trees. 2009.
96. Xie J, Chen Y, Cai G, Cai R, Hu Z, Wang H. Tree visualization by one table (tvBOT): a web application for visualizing, modifying and annotating phylogenetic trees. Nucleic Acids Res. 2023;51(W1):W587–92.

Publisher's Note